

# Iron and Titanium Abundance and Maturity Degree Distribution on the Lunar Nearside

Yurij G. Shkuratov, Vadym G. Kaydash, and Nickolaj V. Opanasenko

*Astronomical Observatory of Kharkov State University, Sumskaya Street 35, Kharkov 310022, Ukraine*

E-mail: shkuratov@ygs.kharkov.ua

Received April 10, 1998; revised September 3, 1998

New digital images of the lunar nearside albedos at 0.42, 0.65, 0.75, and 0.95  $\mu\text{m}$  derived from telescopic data were used to map the abundance and distribution of iron, titanium, and maturity degree on the lunar nearside. Developing the approach by P. Lucey *et al.* (1995, *Science* 268, 1150), a method of separating contributions of the Fe and Ti abundance and maturity degree to spectral properties of the lunar surface is presented. The main objective of the method is an analysis of the 3D correlation diagram of optical characteristics of regolith material with the aim of choosing a coordinate system providing the best correlations of these characteristics with Fe and Ti abundance (data for the Surveyor, Luna, and Apollo landing sites) and with maturity degree (laboratory measurements of lunar samples by E. Fischer and C. Pieters (e.g., 1996, *J. Geophys. Res.* 101, 2225). To find the coordinates, a geometrical optics model of light scattering in particulate media enabling to calculate the absorption coefficient from albedo measurements is used. An analysis of the correlation diagram FeO–TiO<sub>2</sub> provides two maps characterizing optical types of the lunar nearside. In particular, the maps show that the basalts of Mare Serenitatis and Mare Tranquillitatis are not widely extended on the lunar nearside. The maturity degree, parameter  $I_s/\text{FeO}$ , was also mapped. Regions with  $I_s/\text{FeO} \leq 50$  are young craters surrounded by ray systems, whereas the condition  $I_s/\text{FeO} \geq 70$  corresponds to regions associated with Copernicus ejecta, western boundaries of Mare Tranquillitatis and Mare Serenitatis, and a portion of the south highland. The new map of FeO distribution on the lunar nearside was used to study a correlation between iron content and distribution of remanent magnetism over the lunar surface. The relationship obtained has a reverse behavior: the lower the iron content, the higher the magnetism. © 1999 Academic Press

**Key Words:** lunar nearside; optical characteristics of regolith; maturity degree; Fe and Ti abundance.

## INTRODUCTION

Knowledge of compositional structure of the lunar surface can be derived from optical measurements. This is possible due to correlations between optical characteristics and abundance of the main lunar chromophore elements, such as Fe and Ti (e.g., Pieters and McCord 1976, Pieters 1977, 1978, Jaumann 1991).

The optical characteristics depend not only on bulk composition, but also on concentration of finely dispersed metal forms of these elements in upper layers of regolith particles. This concentration is closely related with maturity degree of the regolith (e.g., Pieters 1977, 1978, Morris 1976, 1978). To determine abundance of Fe and Ti, empirical calibrating correlations obtained by means of laboratory studies of lunar regolith samples are usually used. As examples of such correlations, we could remind the “titanium–color” dependence by Charette *et al.* (1974) or the “pyroxenes” curve by Adams (1974).

Recently, a technique for separating the influence of Fe and Ti abundance and maturity degree on spectral properties of the lunar surface has been proposed (Lucey *et al.* 1995, 1996, 1997, 1998a,b, Lucey and Blewett 1997, Blewett *et al.* 1997a,b). In the case of Fe, it is based on a choice of such a system of polar coordinates on the plane of albedo  $A(0.75 \mu\text{m})$  and color-index  $C(0.95/0.75 \mu\text{m})$  that the polar angle and radial coordinate are related to iron content and maturity degree, respectively. For the case of Ti determination, a similar analysis of the diagram  $A(0.75 \mu\text{m})$ – $C(0.42/0.75 \mu\text{m})$  is used (Blewett *et al.* 1997a, Lucey *et al.* 1998a). To choose the proper coordinate systems, data for lunar samples are used. It should be emphasized that the fact of existence of “separating” points on the diagrams is not grounded physically—it is only an empirical fact.

The Lucey *et al.* technique faces a few problems. For example, to derive the maturity degree, one can investigate both diagrams,  $A(0.75 \mu\text{m})$ – $C(0.95/0.75 \mu\text{m})$  and  $A(0.75 \mu\text{m})$ – $C(0.42/0.75 \mu\text{m})$ ; however, these two estimations of maturity degree give different results (Kaydash, 1998). Moreover, both these results are not in a good agreement with an independent maturity determination suggested by Fischer and Pieters (1996). We try here to improve and develop somewhat the approach (Lucey *et al.* 1995, 1996, 1997, 1998a,b, Lucey and Blewett 1997, Blewett *et al.* 1997a,b). Our main idea is to analyze the 3D correlation diagram of parameters closely related with the optical coordinates  $A(0.75 \mu\text{m})$ ,  $C(0.95/0.75 \mu\text{m})$ , and  $C(0.65/0.42 \mu\text{m})$ . The parameters are a result of some nonlinear transformation of the optical coordinates to make separation of composition and maturity more reliable. Moreover, the choice of new coordinates is considered as optimal, when their proper correlations with Fe

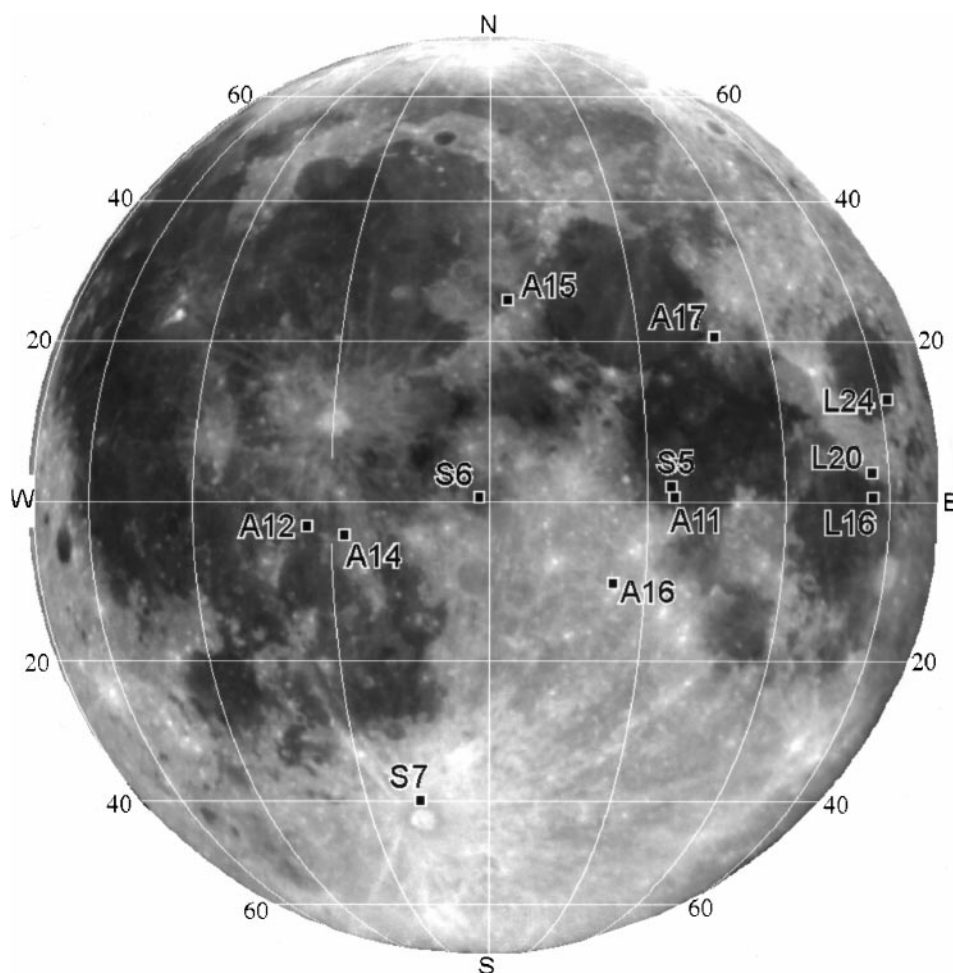


**FIG. 1.** An albedo image of the lunar nearside with the Surveyor, Luna, and Apollo landing sites. The image was obtained by the 70-cm telescope of Kharkov astronomical observatory at a phase angle of about  $6^\circ$ .

and Ti content (data for the Surveyor, Luna, and Apollo landing sites) and with maturity degree (the laboratory measurements of lunar samples by Fischer (1995) and Fischer and Pieters (1996)) are the closest.

#### OPTICAL DATA USED AND NEW APPROACH

To demonstrate our approach, we use digital images (0.42, 0.65, 0.75, and  $0.95 \mu\text{m}$ ) of the lunar nearside derived from telescope data (Opanasenko *et al.* 1996, Shkuratov *et al.* 1997, Opanasenko and Shkuratov 1998). These images were corrected by sets of discrete photometric data (Akimov 1988, Shkuratov *et al.* 1992). The technique of this correction and image calibration was described by Opanasenko *et al.* (1997), Shkuratov *et al.* (1997), and Opanasenko and Shkuratov (1998). A comparison of the corrected images with the lunar spectrophotometric catalog by C. Pieters shows good correlations that confirm the good quality of our data; e.g., the correlation coefficient for the color index  $C(0.65/0.42 \mu\text{m})$  is of about 0.91 for 310 points (Opanasenko *et al.* 1997). Our albedo and colorimetric

images of the lunar nearside are presented in Figs. 1–3. Correlation diagrams of the color index  $C(0.65/0.42 \mu\text{m})$  vs albedo  $A(0.65 \mu\text{m})$  and the color index  $C(0.95/0.75 \mu\text{m})$  vs albedo  $A(0.75 \mu\text{m})$  are given in Figs. 4 and 5, respectively. The diagrams have a structure. For instance, on the diagram  $C(0.95/0.75 \mu\text{m})$ – $A(0.75 \mu\text{m})$ , several clusters are elongated approximately to a point with coordinates  $C = 1.28$ ,  $A = 0.09$ . This fact is important in order to interpret the  $C$ – $A$  diagram by the Lucey *et al.* (1995) approach.

The 3D correlation diagram  $A(0.75 \mu\text{m})$ – $C(0.95/0.75 \mu\text{m})$ – $C(0.65/0.42 \mu\text{m})$  can be analyzed in a similar way. Unfortunately, it is difficult to represent the 3D diagram as a picture; however, this does not prevent its formal analysis by a computer. In this paper we deal with 3D diagram of the parameters closely related with the optical characteristics,  $A(0.75 \mu\text{m})$ ,  $C(0.95/0.75 \mu\text{m})$ , and  $C(0.65/0.42 \mu\text{m})$ .

Usually chemical composition and optical properties of the lunar surface are compared directly, though this should be done with optical properties of the material forming this surface. To derive information on the “material” optical properties from

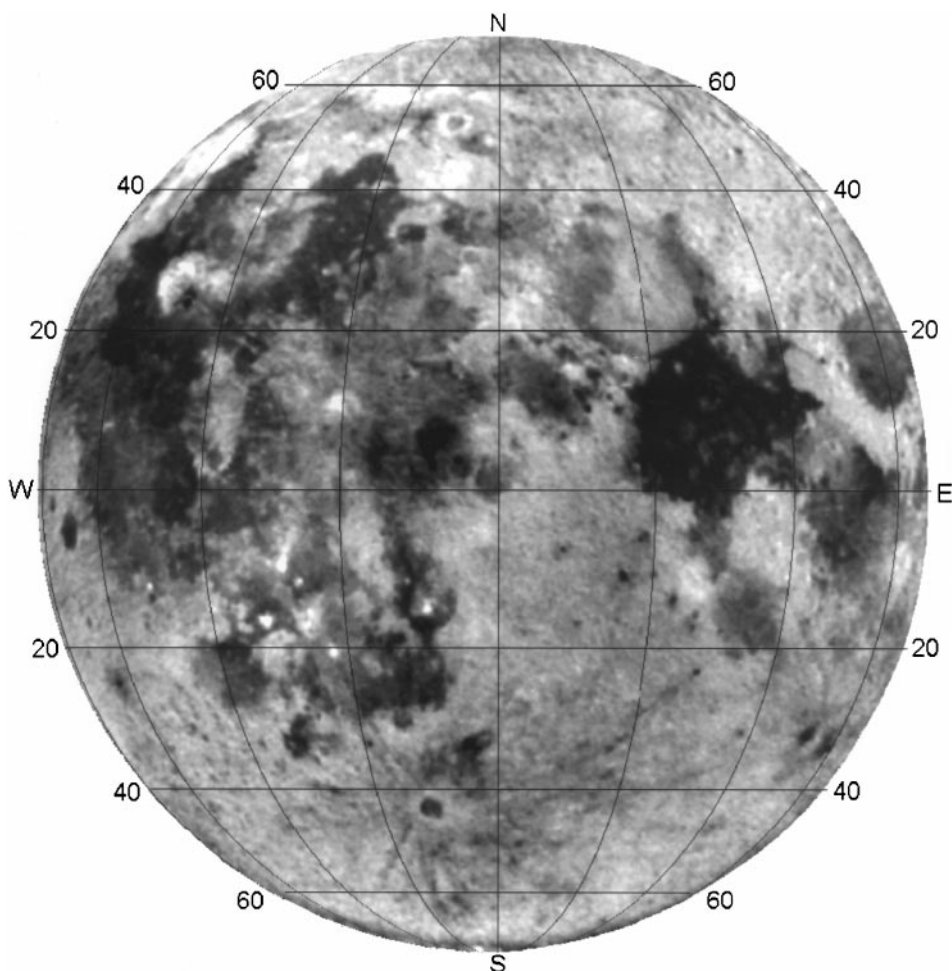


FIG. 2. A color-index (0.65/0.42  $\mu\text{m}$ ) image of the lunar nearside obtained by the method described by Opanasenko *et al.* (1996).

the “usual” optical properties, a geometrical optics model for albedo spectral dependence of regolith-like surfaces (Shkuratov 1987, Shkuratov *et al.* 1998) is used. The model describes light-scattering from particulate surfaces with optical constants  $n$  and  $k$ , the real and imaginary parts of the refractive index. Ray propagating between scatter points is characterized by the absorption coefficient  $\tau = 4\pi kl/\lambda$ , where  $l$  is the average length of light propagation in a particle between internal reflections. The model is formally one-dimensional, though it takes into account some properties of the 3D case. In particular, it uses the coefficient  $\mu$  which is the volume fraction of the regolithic medium filled with particles. An important characteristic of the model is its invertibility; i.e., the function  $k(\lambda)$  can be found if the spectral albedo  $A(\lambda)$  is known and estimates for the parameters  $n$ ,  $l$ , and  $\mu$  are available. The main relationships of this model are (Shkuratov *et al.* 1998)

$$k(\lambda) = -\frac{\lambda}{4\pi \cdot l} \ln \left[ \frac{b}{a} + \sqrt{\left(\frac{b}{a}\right)^2 - \frac{c}{a}} \right], \quad (1)$$

where

$$\begin{aligned} a &= (1 - R_e)(1 - R_i) \left( \frac{[1 - A(\lambda)]^2}{2A(\lambda)} R_i + \mu(1 - R_e) \right), \\ b &= \frac{[1 - A(\lambda)]^2}{2A(\lambda)} R_b R_i + \frac{\mu}{2} (1 - R_e)^2 (2 - R_i) \\ &\quad - (1 - R_e)(1 - \mu R_b), \\ c &= \frac{[1 - A(\lambda)]^2}{A(\lambda)} R_b - 2(1 - R_e)(1 - \mu R_b) + \mu(1 - R_e)^2, \\ R_b &= (0.28 \cdot n - 0.20) R_e, \\ R_e &= (n - 1)^2 / (n + 1)^2 + 0.05, \\ R_i &= 1.04 - 1/n^2. \end{aligned}$$

Thus, using digital albedo (0.42, 0.65, 0.75, 0.95  $\mu\text{m}$ ) images we found the values  $k(0.42 \mu\text{m})$ ,  $k(0.65 \mu\text{m})$ ,  $k(0.75 \mu\text{m})$ , and  $k(0.95 \mu\text{m})$  by means of formula (1). The following values of model parameters are used:  $n = 1.5$ ,  $\mu = 0.5$ , and  $l = 50 \mu\text{m}$ .

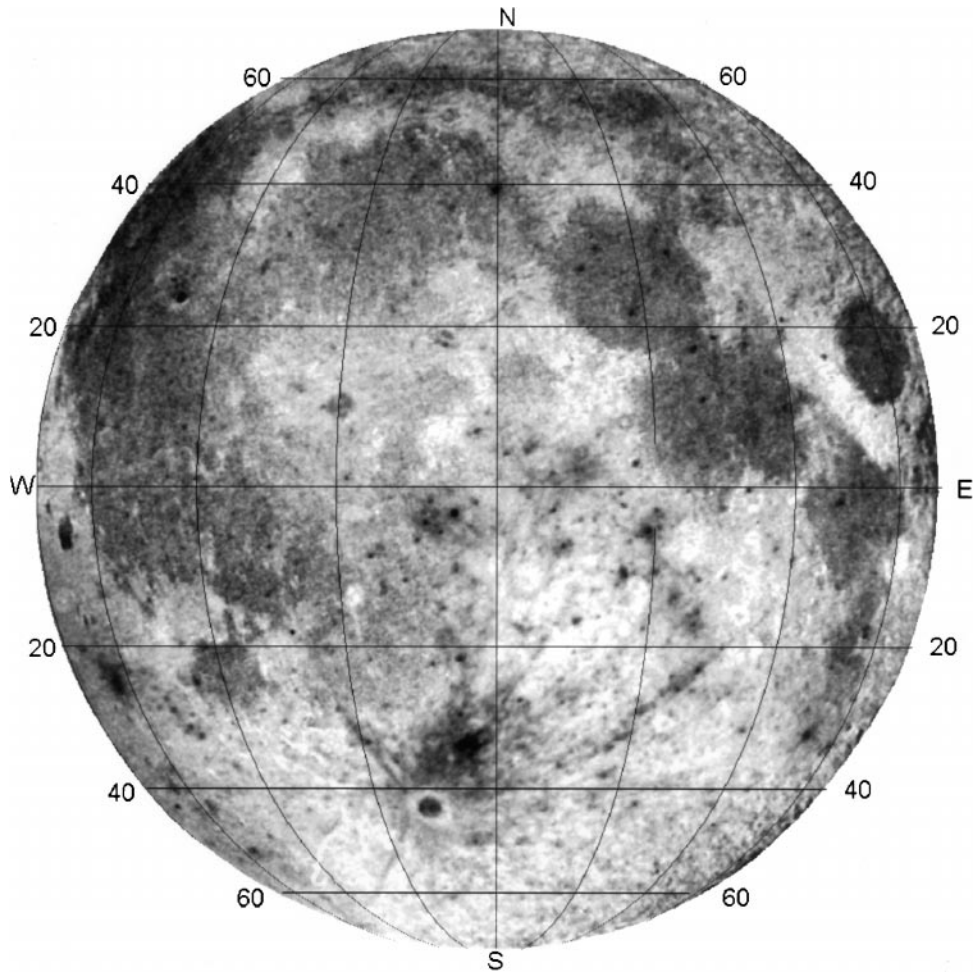


**FIG. 3.** A color-index ( $0.95/0.75 \mu\text{m}$ ) image of the lunar nearside by the method described by Opanasenko and Shkuratov (1998).

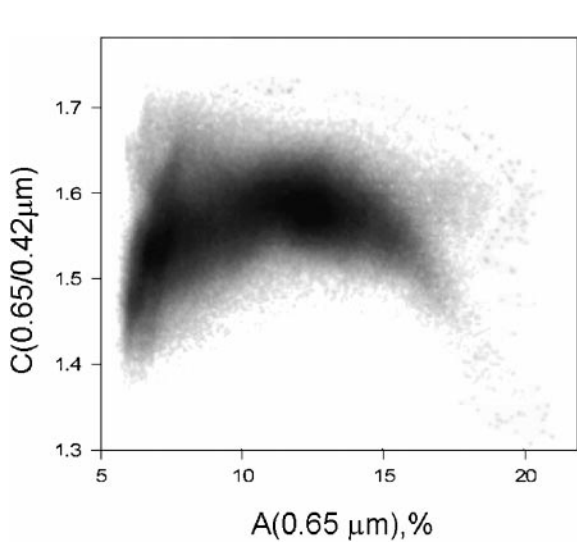


**FIG. 4.** A correlation diagram  $A(0.65 \mu\text{m})-C(0.65/0.42 \mu\text{m})$  of the lunar nearside.

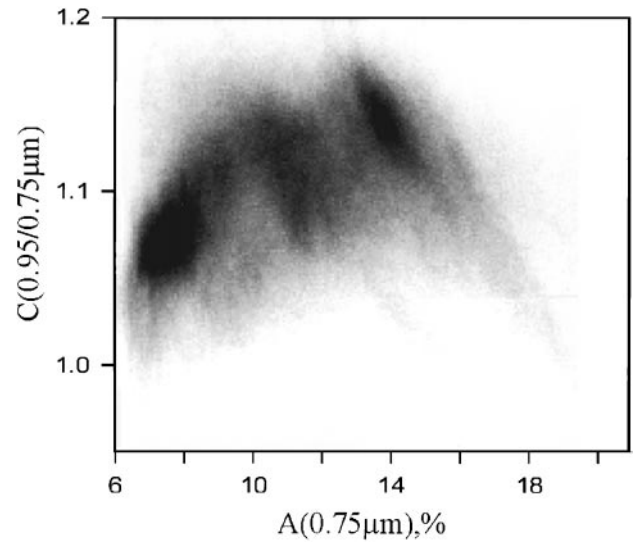


**FIG. 5.** A correlation diagram  $A(0.75 \mu\text{m})-C(0.95/0.75 \mu\text{m})$  of the lunar nearside.

These values are rather typical for lunar regoliths (Heiken *et al.* 1991).

Further, we use the 3D diagram  $k(0.42 \mu\text{m})-C_k(0.42/0.65 \mu\text{m})-D_k(0.95 \mu\text{m})$ , where  $C_k(0.42/0.65 \mu\text{m})=k(0.42 \mu\text{m})/k(0.65 \mu\text{m})$  and  $D_k(0.95 \mu\text{m})$  is a depth parameter of the  $1\text{-}\mu\text{m}$  absorption band:  $D_k(0.95 \mu\text{m})=k(0.95 \mu\text{m})/k_c(0.95 \mu\text{m})$ , the value  $k_c(0.95 \mu\text{m})$  being an absorption coefficient in continuum. It was found by linear extrapolation of the function  $k(\lambda)$  using three wavelengths, 0.42, 0.65, and  $0.75 \mu\text{m}$ . Unlike the ratio  $k(0.75 \mu\text{m})/k(0.95 \mu\text{m})$ , the parameter  $D_k(0.95 \mu\text{m})$  depends only slightly on the general slope of adsorption spectra.

We search for such a new coordinate system—a linear combination of the parameters  $k(0.65 \mu\text{m})$ ,  $C_k(0.42/0.65 \mu\text{m})$ , and  $D_k(0.95 \mu\text{m})$ —that these new coordinates show the best proper correlations with FeO and  $\text{TiO}_2$  abundance and maturity degree. This is the crucial point of our approach. The search of the optimum was carried out by simple sorting out in computer memory.

The following oblique-angled coordinates satisfy the mentioned optimal condition  $D_k(0.95 \mu\text{m})$ ,  $C_k(0.42/0.65 \mu\text{m})$ , and  $G$ , where  $G=k(0.65 \mu\text{m}) \times 10^5 + 5 \times D_k(0.95 \mu\text{m})$ , if we use chemical data presented in Table I. Thus, it turns out that two

**TABLE I**  
**Chemical Data for Soils from the “Apollo,” “Luna,” and “Surveyor” Landing Sites**

Landing site	TiO <sub>2</sub> (%)	<i>t</i> (%)	FeO (%)	<i>f</i> (%)	References
Apollo 11	7.40	25	15.8	15	Nawa and Philpotts 1979, Heiken <i>et al.</i> 1991, King 1976, Florensky <i>et al.</i> 1981
Apollo 12	2.68	10	15.7	5	Nawa and Philpotts 1979, Heiken <i>et al.</i> 1991, King 1976, Florensky <i>et al.</i> 1981
Apollo 14	1.72	20	10.4	15	Nawa and Philpotts 1979, King 1976, Florensky <i>et al.</i> 1981
Apollo 15 (mare)	1.64	30	15.2	20	Nawa and Philpotts 1979, Heiken <i>et al.</i> 1991, Florensky <i>et al.</i> 1981
Apollo 15 (highland)	0.29		7.0		Florensky <i>et al.</i> 1981
Apollo 16	0.55		5.0		Nawa and Philpotts 1979, Florensky <i>et al.</i> 1981, Heiken <i>et al.</i> 1991
Apollo 17 (mare)	9.50		15.0		LSPET 1973, Heiken <i>et al.</i> 1991
Apollo 17 (highland)	0.90	60	8.1	50	LSPET 1973
Luna 16	3.36	10	16.7	15	Florensky <i>et al.</i> 1981, Heiken <i>et al.</i> 1991
Luna 20	0.47	20	7.4	15	Nawa and Philpotts 1979, Florensky <i>et al.</i> 1981, Heiken <i>et al.</i> 1991
Surveyor 5	7.60	30	12.1	15	Mason and Melson 1970
Surveyor 6	3.50	30	12.4	15	Mason and Melson 1970
Surveyor 7	0.50	30	5.5	15	Mason and Melson 1970
Luna 24	1.15	20	20.6	15	Florensky <i>et al.</i> 1981, Heiken <i>et al.</i> 1991

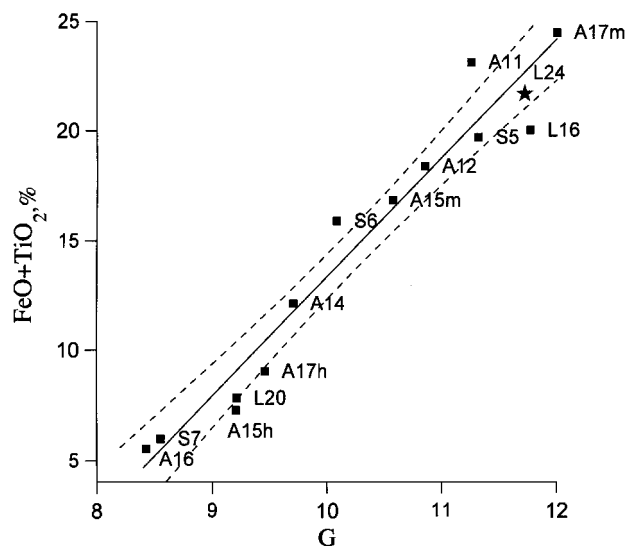


**FIG. 6.** Abundance of  $(\text{FeO} + \text{TiO}_2)$  vs parameter  $G=k(0.65) \times 10^5 + 5 \times D_k(0.95 \mu\text{m})$  for the Surveyor, Luna, and Apollo landing sites. The data for Luna 24 were excluded from the statistical analysis.

coordinates,  $C_k(0.42/0.65 \mu\text{m})$ ,  $D_k(0.95 \mu\text{m})$ , remain the same after the search. They have clear physical sense. The first parameter correlates with Ti abundance and the second one with maturity degree. The third new parameter is  $G$ —a formal parameter related basically to Fe content.

In Table I data on average FeO and  $\text{TiO}_2$  abundance for the landing sites of the Apollo 11, 12, and 14–17 missions and the spacecrafts Surveyor 5–7 and Luna 16–20 are presented. We incorporated from literature only data for regoliths. Besides, using different sources we found uncertainties in estimation of these characteristics:  $t = \Delta(\text{TiO}_2)/(\text{average TiO}_2 \text{ abundance})$

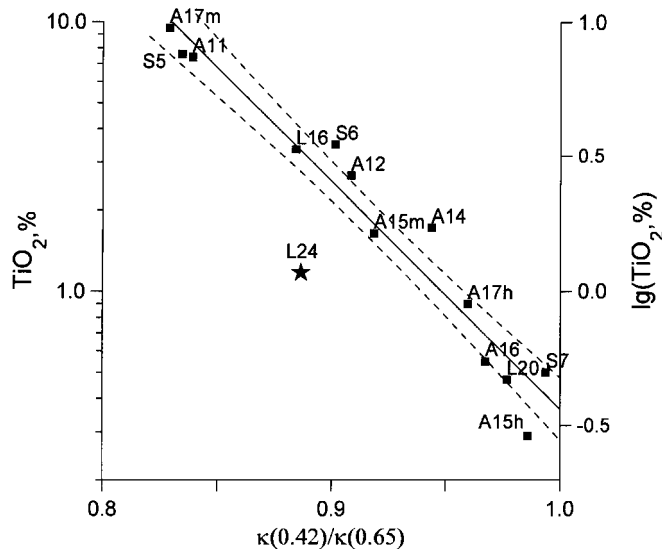


**FIG. 7.** Abundance of  $\text{TiO}_2$  vs  $k(0.42/0.65 \mu\text{m})$  for the Surveyor, Luna, and Apollo landing sites. The data for Luna 24 were excluded from the statistical analysis.

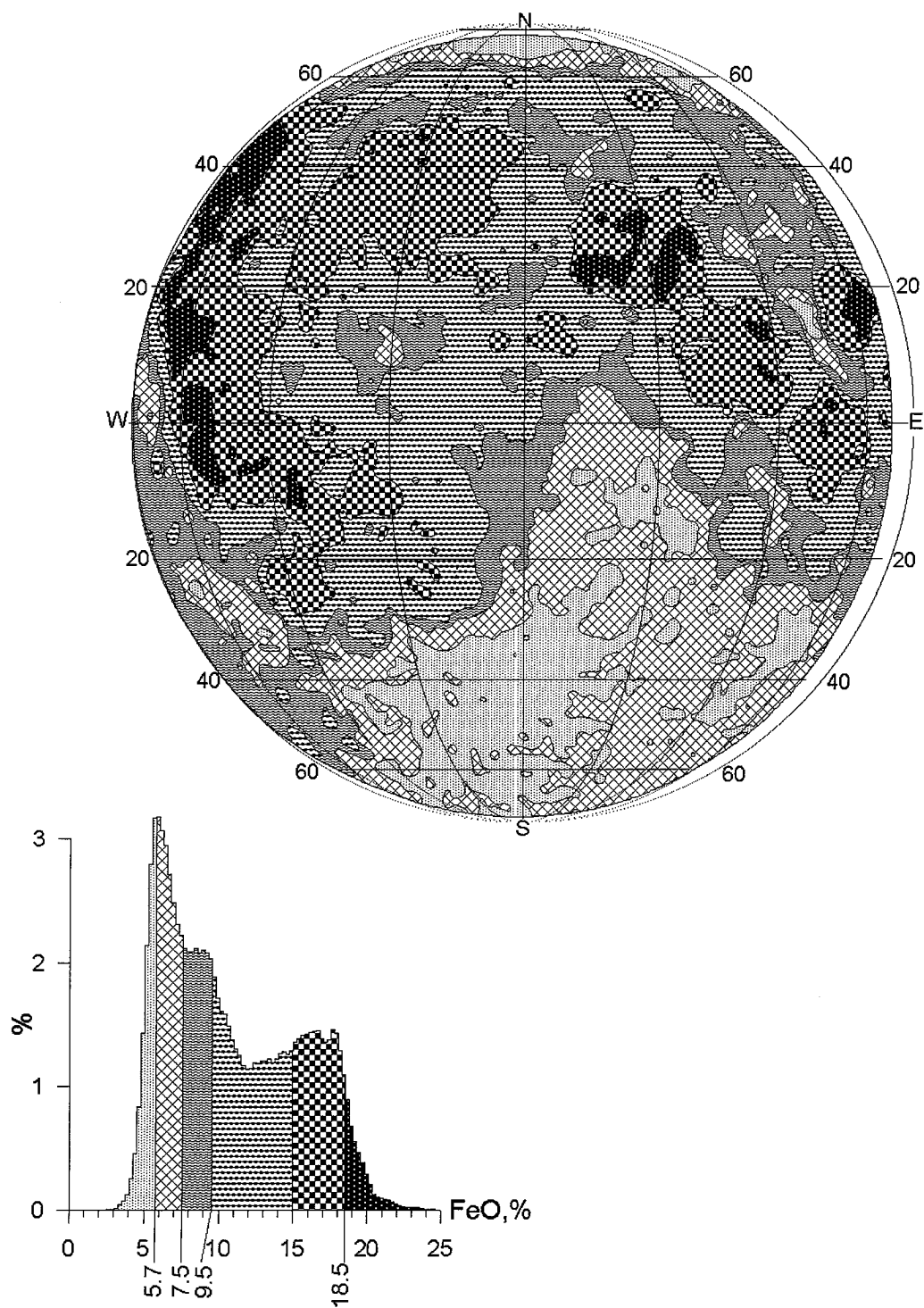


FIG. 8. A map of FeO abundance on the lunar nearside and statistical histogram. The calibrations (3) and (4) were used.

and  $f = \Delta(\text{FeO}) / (\text{average FeO abundance})$ , where  $\Delta(\text{FeO})$  and  $\Delta(\text{TiO}_2)$  are dispersions of data which can be caused by both measurement errors (the Surveyor data) and diversity of samples (the Apollo missions). We realize that one can use another literature sources and will have slightly different average FeO

and  $\text{TiO}_2$  abundance for the landing sites. However, despite this, it is necessary to develop this approach, improving initial data step by step.

Although we presented data for the Luna 24 landing site in Table I and some figures, these data were excepted from our

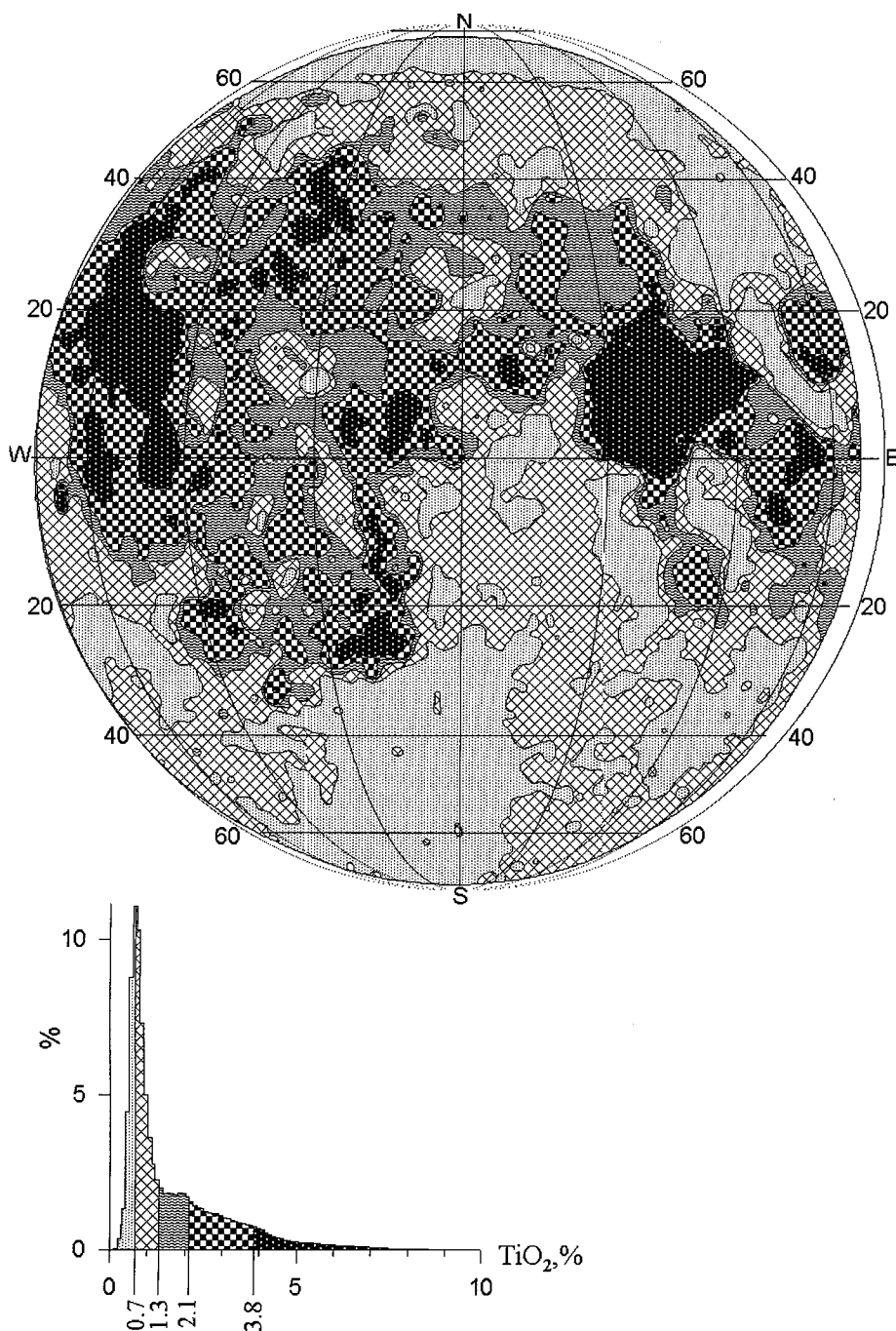


FIG. 9. A map of  $\text{TiO}_2$  abundance on the lunar nearside and statistical histogram. The calibration (3) was used.

statistical analysis, since the landing site is probably not representative for the region (Ryder 1977, Blewett *et al.* 1997a, Lucey *et al.* 1998a).

In Figs. 6 and 7, the “optimal” calibration dependences for  $(\text{FeO} + \text{TiO}_2) - G$  and  $\log(\text{TiO}_2) - C_k (0.65/0.42 \mu\text{m})$  are shown. As one can see, the correlations are rather close. The linear regression analysis gives the correlation coefficients of about

0.97 in both the cases. The regression equations are

$$(\text{FeO} + \text{TiO}_2[\%]) = 5.43 \cdot G - 40.94, \quad (2)$$

$$\log(\text{TiO}_2[\%]) = -8.45 \cdot C_k + 8.01. \quad (3)$$

Confidence level curves of the correlations are also plotted on

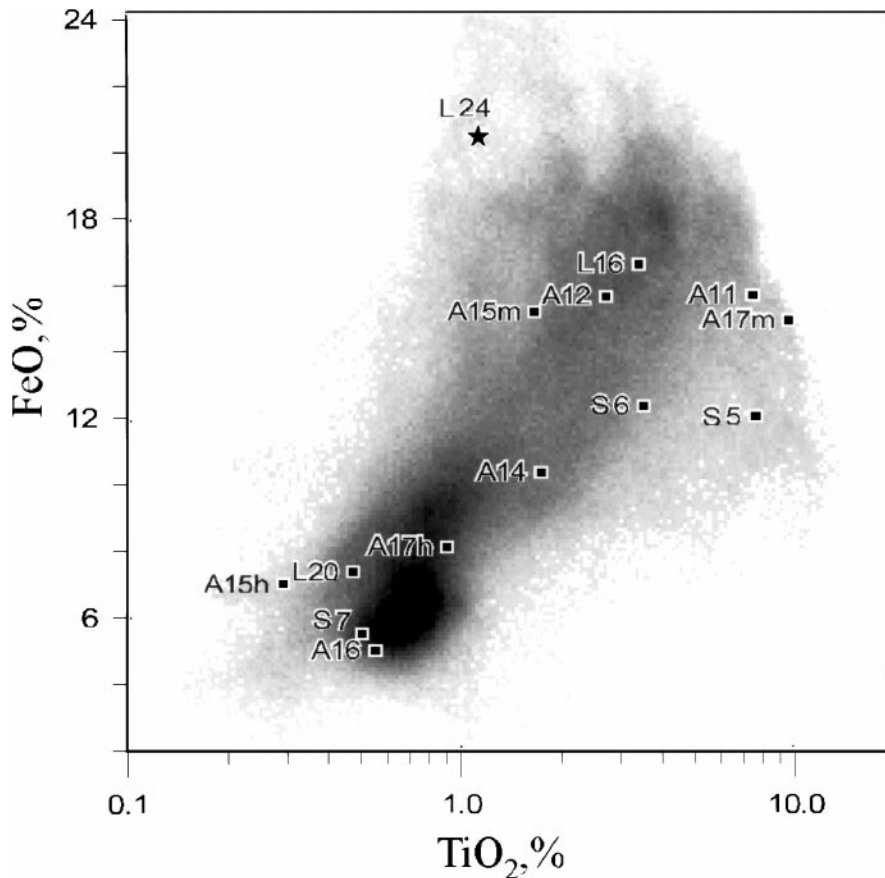


FIG. 10. A correlation diagram FeO–TiO<sub>2</sub> of the lunar nearside and data for the Surveyor, Luna, and Apollo landing sites.

Figs. 6 and 7. As can be expected, distance between these curves increases for the ends of the plot.

In this analysis we involved the maturity parameter  $I_s/\text{FeO}$  defined by Morris (1976, 1978). Here  $I_s$  is the concentration of reduced single-domain iron formed by effects of cosmogenic reworking of the lunar surface. The parameter  $I_s$  is measured by the ferromagnetic resonance method.

For maturity degree calibration, we used spectral data by Fischer (1995) and Fischer and Pieters (1996) for 10 lunar samples with known parameter  $I_s/\text{FeO}$ . We transformed the laboratory optical data in our photometric system (Opanasenko *et al.* 1997, Opanasenko and Shkuratov 1998). We used for this the ratio of telescopic albedo for the Apollo 16 landing site and laboratory reflectance of a typical soil from the site at  $\lambda = 0.65 \mu\text{m}$  (Kaydash 1998). We obtained the following equation for the maturity degree parameter  $I_s/\text{FeO}$ :

$$\log(I_s/\text{FeO}) = 244.8k(0.65 \mu\text{m}) - 4.896D_k(0.95 \mu\text{m}) + 7.175. \quad (4)$$

Thus, the FeO and TiO<sub>2</sub> calibrations were obtained by telescopic spectra and laboratory chemical data for the landing sites. To obtain the  $I_s/\text{FeO}$  calibration, we used spectral data for 10 lunar samples with known maturity degree.

So, in order to use our approach, it is necessary:

- (1) to present our data for  $A(0.42 \mu\text{m})$ ,  $A(0.65 \mu\text{m})$ ,  $A(0.75 \mu\text{m})$ , and  $A(0.95 \mu\text{m})$  in the photometric system by Opanasenko *et al.* (1997) and Opanasenko and Shkuratov (1998);
- (2) to find the parameters  $k(0.65 \mu\text{m})$ ,  $C_k(0.42/0.65 \mu\text{m})$ , and  $D_k(0.95 \mu\text{m})$  by the model (see formula (1));
- (3) to calculate the values FeO, TiO<sub>2</sub>, and  $I_s/\text{FeO}$  using Eqs. (2)–(4).

## RESULTS

We describe here new maps of FeO and TiO<sub>2</sub> abundance and maturity degree for the lunar nearside. The correlation diagram FeO–TiO<sub>2</sub> and results of its cluster analysis are also presented. Besides, the correlation between our data on iron abundance and data on remanent magnetism by Lin *et al.* (1976) is studied.

*FeO and TiO<sub>2</sub> abundance.* Making use of the calibrations (2) and (3), maps of Fe and Ti abundance on the lunar nearside were produced (Figs. 8 and 9). As one can see, the ray systems of bright craters are largely quenched, though sometimes they still show up. For instance, the iron image (Fig. 8) shows that Tycho ejecta have a somewhat lower Fe content than surroundings. This is not yet observed in new Lunar Prospector data

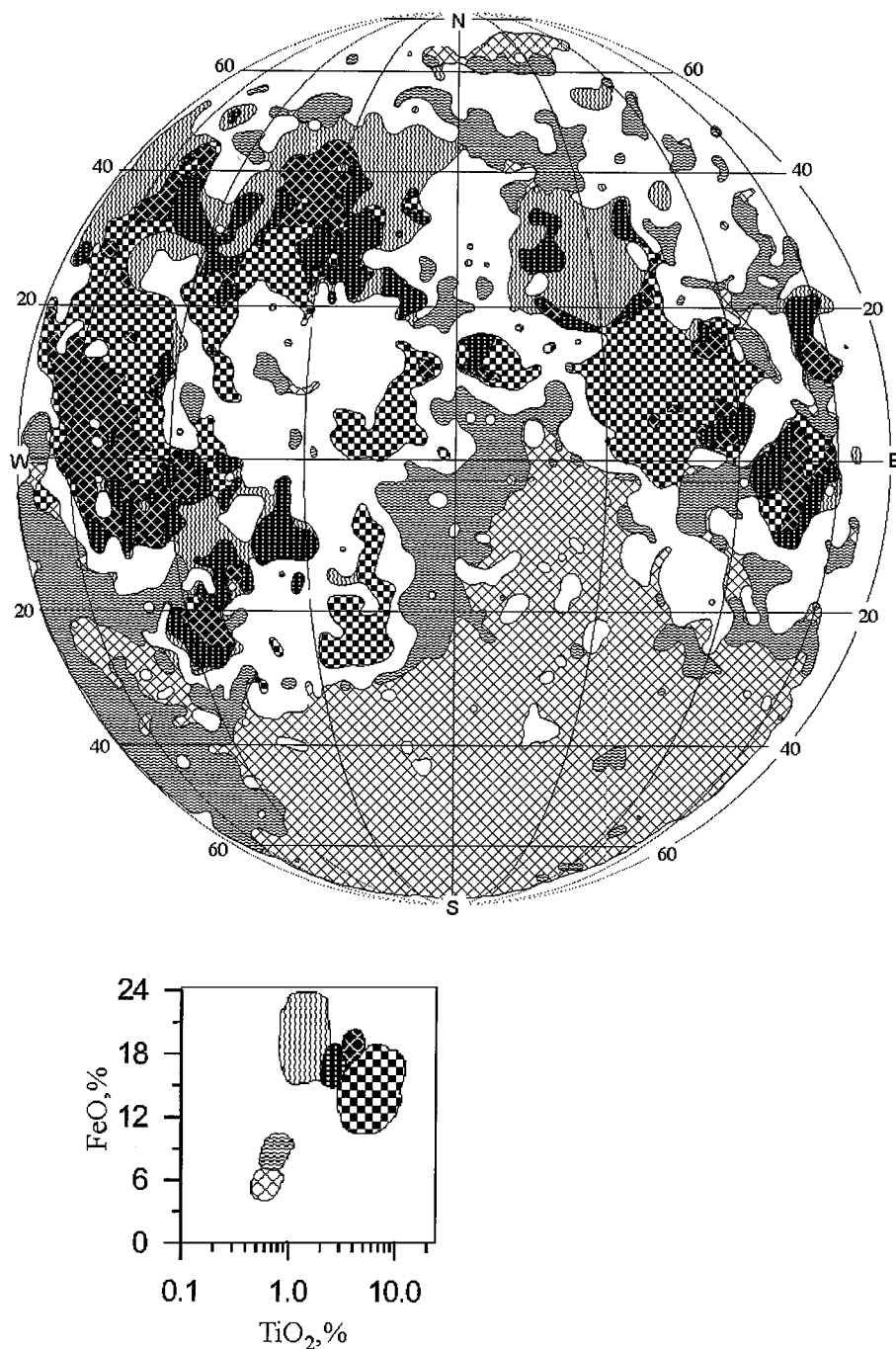


FIG. 11. A map of optical types of the lunar nearside surface. Cluster analysis for the correlation diagram FeO–TiO<sub>2</sub> was used.

(Lucy 1998, pers. commun.). Thus, probably, this feature is a result of the approximateness of our technique.

In Figs. 8 and 9, the frequency histograms are also presented. The histogram of Fe abundance is bimodal. The maxima of the modes lie near 6 and 17%. This is in a good agreement with the results for the lunar nearside obtained by Clementine data (Lucy *et al.* 1998a). The frequency histogram for titanium has only one maximum and is very asymmetric. The maximum of

the distribution is near 0.7%. Using data presented above we have studied the relationship for FeO and TiO<sub>2</sub>. Slicing of both histograms is largely arbitrary, though we tried to make some grade equalization and to coordinate this with general look of the histograms.

The correlation diagram FeO–TiO<sub>2</sub> for the lunar nearside is given in Fig. 10. It shows the correlation to be rather high with the correlation coefficient 0.81. The regression equation is as

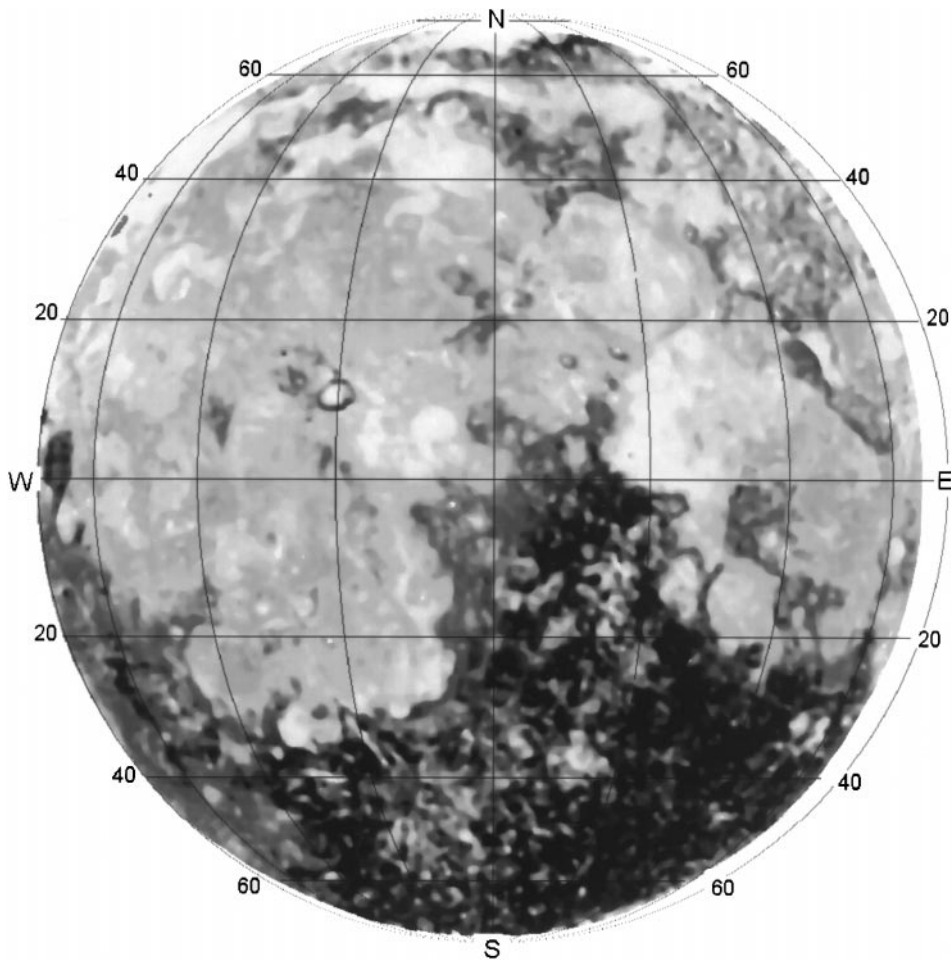


**FIG. 12.** An image of lunar surface typicalness of FeO and TiO<sub>2</sub> combinations. Dark hues correspond to more probable combinations of FeO and TiO<sub>2</sub> values.

follows:

$$\log(\text{TiO}_2[\%]) = 0.06 \cdot (\text{FeO}[\%]) - 0.54. \quad (5)$$

On the diagram FeO–TiO<sub>2</sub>, the high-albedo part is presented by two clusters with diffuse boundaries. Unlike this, the low-albedo part exhibits a richer structure. We see also that the Luna 24 landing site has really an unusual combination of FeO and TiO<sub>2</sub> abundance.

The diagram can be used to classify the lunar surface. Two maps of optical types of the lunar nearside surface are presented in Figs. 11 and 12. The first of them is a result of cluster analysis of the diagram FeO–TiO<sub>2</sub>, in which six clusters were selected. The most interesting ones are two clusters contributed by Mare Serenitatis and Mare Tranquillitatis. The first cluster has got higher FeO but lower TiO<sub>2</sub> abundance and the second one is characterized by the opposite combination.

The second map (Fig. 12) shows a distribution of the parameter which we have named “exoticness” (Shkuratov *et al.* 1997). The parameter presents probability of meeting a combination of values of FeO and TiO<sub>2</sub> abundance. Dark tones of the map

(image) correspond to more probable combinations of FeO and TiO<sub>2</sub> abundance. For example, most typical combinations of FeO and TiO<sub>2</sub> abundance can be met in the south highland rounding the crater Tycho. Basalts of Mare Serenitatis and Mare Tranquillitatis are rare materials from the standpoint of this analysis. It is interesting that the Copernicus ray system disappears on the image, i.e., materials of the region have no high typicalness.

*Maturity degree.* Presented in Fig. 13 is an attempt to map the maturity degree parameter  $I_s/\text{FeO}$  using Eq. (4). Dark shade in the  $I_s/\text{FeO}$  map shows young craters and their ejecta (immature soils), e.g., the crater Tycho and its ray system. The crater Copernicus shows up too, but its ray system has rather high maturity. The mare/highland boundary is practically not seen on the lunar nearside in parameter  $I_s/\text{FeO}$ . That is in a good agreement with results of laboratory studies of lunar samples (Morris 1976, 1978), which have shown that the correlation between the parameters  $I_s/\text{FeO}$  and iron content does not exist for mare samples as well as for highland ones. It means that lunar images in the parameter  $I_s/\text{FeO}$  should not feel the mare/highland boundary. Bright hues of the map show zones of high maturity. These

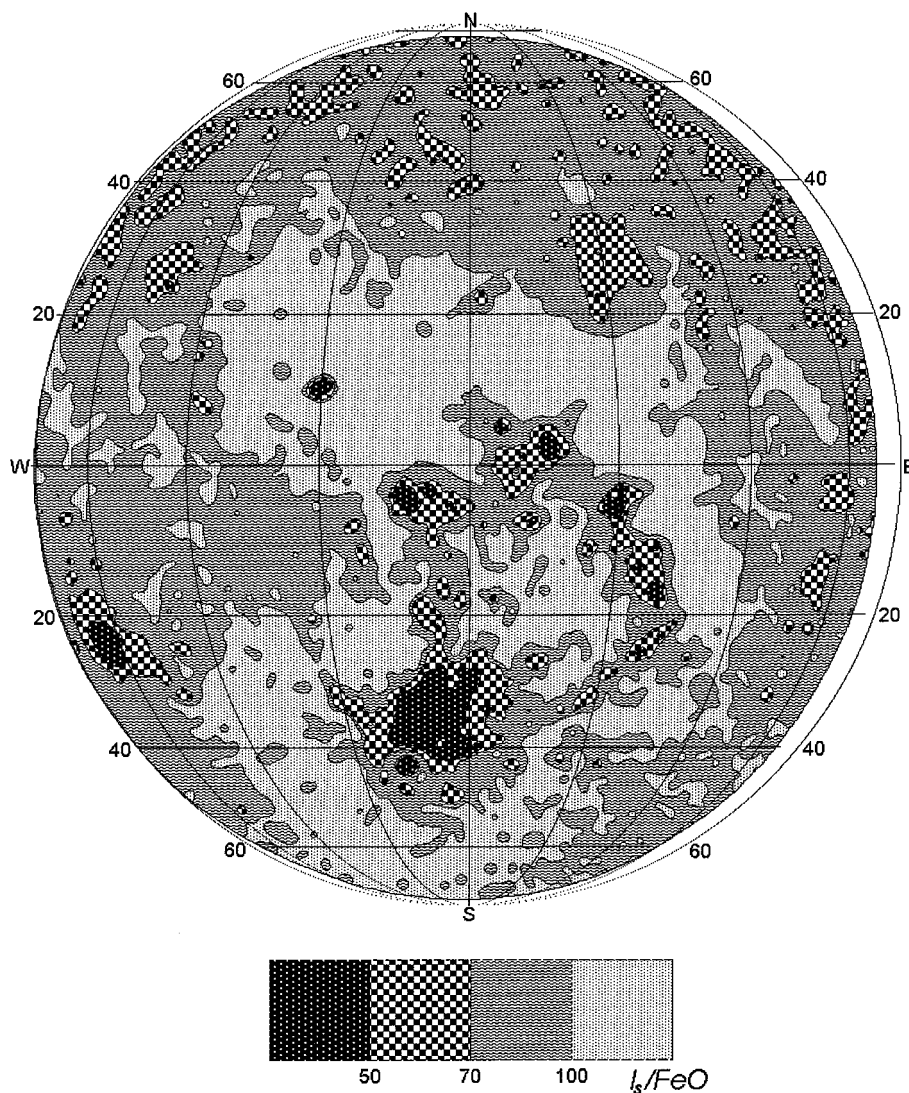


FIG. 13. An  $I_s/\text{FeO}$  map of the lunar nearside. The calibration (4) was used.

zones include the Copernicus ray system, the southwestern border of Mare Serenitatis, the western part of Mare Tranquillitatis and Mare Nectaris, and a portion of the southern highland. The high-maturity zones correlate with morphological features of the lunar surface. Note that the map given in Fig. 13 is in a good agreement with the maturity distribution presented by Lucey *et al.* (1998b).

*Correlation between iron content and remanent magnetism.* Investigations of the correlation between lunar remanent magnetism and some chemical elements abundance (mainly reduced iron) are important for understanding the present structure and evolution of the Moon interior. Available data on the correlation are discrepant. Thus, the correlation is not found in the research by Soderblom *et al.* (1977), which is devoted to studies of relation between lunar remanent magnetism (electron scattering data) and iron content ( $\gamma$ -spectroscopy data with low spatial res-

olution). However, the work by Metzger *et al.* (1977) shows that a weak dependence exists.

In this paper, our map of FeO abundance and the map of radial component of lunar remanent magnetic field (Lin *et al.* 1976) are used to study this problem. The map by Lin *et al.* (1976) has been derived from the measurements of 0.5 Kev electrons backscatter by the lunar surface during Apollo 15 and 16 experiments. According to these data, the magnetic field on the Moon nearside varies from 0.75 to 6.0 gamma. The resolution of this map is a few tens of kilometers. The data on iron content described above are used to prepare statistical distributions of iron content for all levels of the remanent magnetism map. The results are presented in Fig. 14. A tendency of increasing small FeO content contribution when the remanent magnetism increases is clearly seen. It should be emphasized that having the new map of FeO abundance we used much more data than Soderblom *et al.* (1977).

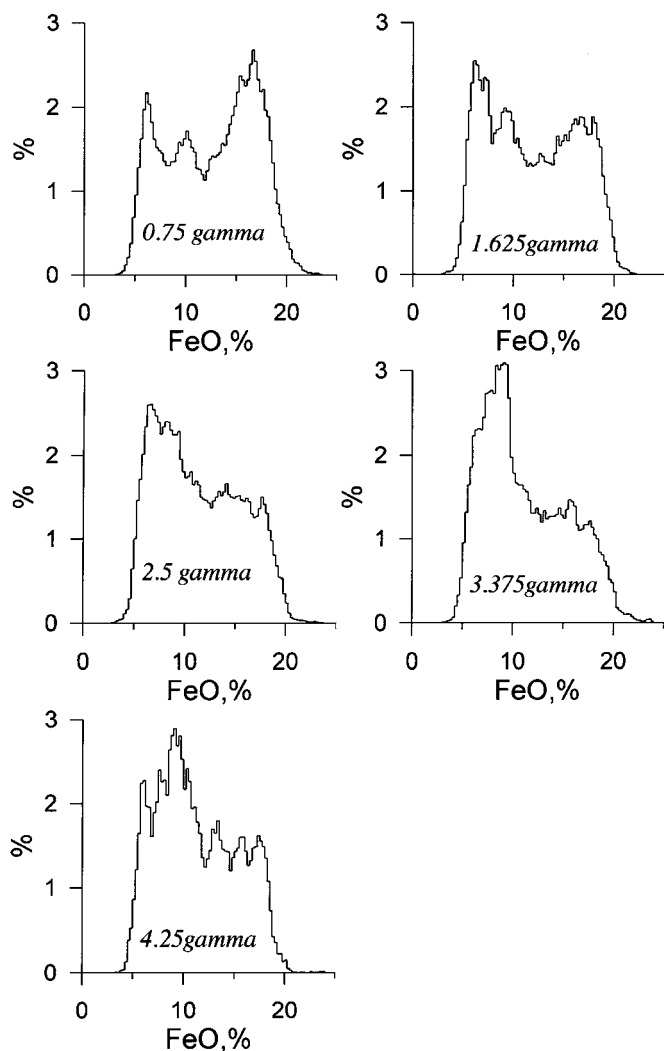


FIG. 14. A correlation between Fe abundance (our data) and remanent magnetism data by Lin *et al.* (1976).

The result obtained looks strange: it would be reasonable to expect that the amount of reduced iron has to increase when  $\text{Fe}^{2+}$  ion content increases, and this fact should give a direct correlation between magnetism and iron content, which is the opposite to that observed. However, this discrepancy may be explained as follows. Regardless of the nature of the source (internal or external), the duration of activity of the lunar rocks magnetism source was short; therefore, more ancient (highland) lunar rocks probably underwent stronger magnetization than mare basalts formed during the source attenuation (Taylor 1972).

### CONCLUSION

The main purpose of the work is achieved: the problem of simultaneous determination of the Fe and Ti contents and maturity degree by means of albedo measurements in four spectral bands is resolved in the first approximation. The most impor-

tant aspect of our approach is a computer formal analysis of the 3D correlation diagram of the optical characteristics of regolith material in order to choose a coordinate system providing the best calibrating correlations of these characteristics with Fe and Ti abundance and with maturity degree parameter  $I_s/\text{FeO}$ . To find the coordinates, we use the geometrical optics model of light-scattering in particulate media enabling calculations of the absorption coefficient from albedo measurements.

This approach allows us to map FeO and  $\text{TiO}_2$  abundance on the lunar nearside. The FeO distribution histogram turns out to be bimodal, whereas the titanium one is monomodal and sharply asymmetric. These results are in a good agreement with the data by Lucey *et al.* (1998a,b).

The correlation diagram FeO– $\text{TiO}_2$  is analyzed and two maps characterizing optical types of the lunar nearside are presented. In particular, the maps show, the basalts of Mare Serenitatis and Mare Tranquillitatis to be not widely extended on the lunar nearside.

Our investigations show that there is a weak correlation between FeO abundance and remanent magnetism. The relationship obtained has a reverse behavior: the lower the iron content, the higher the remanent magnetism. This confirms the data by Metzger *et al.* (1977) who used  $\gamma$ -ray data for estimation of Fe distribution.

The parameter  $I_s/\text{FeO}$  was mapped. Regions with  $I_s/\text{FeO} \leq 50$  are young craters surrounded by ray systems. While the inequality  $I_s/\text{FeO} \geq 70$  corresponds to regions associated with Copernicus ejecta, the western boundaries of Mare Tranquillitatis and Mare Serenitatis, and some portion of south highland.

This approach will be applied to Clementine data including calibrations derived from individual sampling station data of the Apollo 15, 16, and 17 landing sites, as has been proposed by Blewett *et al.* (1997a) and Lucey *et al.* (1998a).

### ACKNOWLEDGMENTS

Authors are very grateful to Paul Lucey and Patrick Pinet, who made a very deep analysis of the paper. This work was supported by CRDF Grant UG2-295.

### REFERENCES

- Adams, J. B. 1974. Visible and near-infrared diffuse reflectance spectra of pyroxenes as applied to remote sensing of solid objects in the Solar System. *J. Geophys. Res.* **79**, 4829–4836.
- Akimov, L. A. 1988. *Studies of the Lunar Surface Scattering Low*. Doctor of Sciences thesis, Astron. Obs. of Kharkov Univ. Kharkov.
- Blewett, D. T., P. G. Lucey, B. R. Hawke, and B. L. Jolliff 1997a. Clementine images of the lunar sample-return station: Refinement of  $\text{TiO}_2$  mapping techniques. *J. Geophys. Res.* **102**, 16,319–16,325.
- Blewett, D. T., P. G. Lucey, B. R. Hawke, and B. L. Jolliff 1997b. FeO mapping of the Moon: Refinement using images of the sample-return stations. *Lunar Planet. Sci. Conf. 28th*, 122. [Abstract]
- Charette, M., T. B. McCord, C. Pieters, and J. B. Adams 1974. Application of remote spectral reflectance measurements to lunar geology classification and determination of titanium content of lunar soils. *J. Geophys. Res.* **79**, 1605–1613.

- Fischer, E. M. 1995. *Quantitative Compositional Analysis of the Lunar Surface from Reflectance Spectroscopy: Iron, Aluminium, and a Model for Removing the Optical Effects of Space Weathering*. Ph.D. thesis, Brown Univ. Providence, RI.
- Fischer, E., and C. Pieters 1996. Composition and exposure age of the Apollo 16 Cayley and Descartes regions from Clementine data: Normalizing the optical effect of space weathering. *J. Geophys. Res.* **101**, 2225–2234.
- Florensky, K. P., and 12 colleagues 1981. *Essays of Comparative Planetology* (V. L. Barsukov, Ed.). Nauka Press, Moscow. [in Russian]
- Heiken, G., D. Vaniman, and B. French 1991. *Lunar Source-Book*. Cambridge Univ. Press, New York.
- Jaumann, R. 1991. Spectral–chemical analysis of lunar surface materials. *J. Geophys. Res.* **96**, 22,793–22,807.
- Kaydash, V. G. 1998. *Prognosis of Chemical Composition and Determination of Surface Type for the Lunar Nearside*. Ph.D. thesis, Kharkov Univ., Kharkov.
- King, E. 1976. *Space Geology (an Introduction)*. Wiley, New York.
- Lin, R. P., K. A. Anderson, R. Bush, R. E. McGuire, and J. E. McCoy 1976. Lunar surface remanent magnetic fields detected by the electron reflection method. *Proc. Lunar Planet. Sci. Conf. 7th*, 2691–2703.
- LSPET (Lunar Sample Preliminary Examination Team) 1973. Apollo 17 lunar samples. Chemical and petrographic description. *Science* **183**, 659–672.
- Lucey, P., and D. Blewett 1997. Some issues related to lunar FeO and TiO<sub>2</sub> multispectral mapping. *Lunar Planet. Sci. 28th*, 841–842. [Abstract]
- Lucey, P., D. Blewett, and B. Hawke 1998a. FeO and TiO<sub>2</sub> concentrations in the south Pole-Aitken basin: Implication for mantle composition and basin formation. *J. Geophys. Res. (Planets)* **103**, 3701–3708.
- Lucey, P., D. Blewett, and J. Johnson, *et al.* 1996. Lunar titanium content from UVVIS measurements. *Lunar Planet. Sci. 27th*, 781–782. [Abstract]
- Lucey, P., G. Taylor, and B. Hawke 1998b. Global imaging of maturity: Results from Clementine and lunar sample studies. *Lunar Planet. Sci. 29th*, 1356. [Abstract]
- Lucey, P., G. Taylor, and E. Malaret 1995. Abundance and distribution of iron on the Moon. *Science* **268**, 1150–1153.
- Lucey, P., G. Taylor, and E. Malaret 1997. Global abundance of FeO on the Moon: Improved estimates from multispectral imaging and comparisons with the lunar meteorites. *Lunar Planet. Sci. 28th*, 850–851. [Abstract]
- Mason, B., and W. Melson 1970. *The Lunar Rocks*. Wiley, New York.
- Metzger, A. E., R. P. Lin, and C. T. Russel 1977. On a correlation between surface remanent magnetism and chemistry for the lunar frontside and limbs. *Proc. Lunar Planet. Sci. Conf. 8th*, 1187–1190.
- Morris, R. 1976. Surface exposure indices of lunar soils: A comparative FMR study. *Proc. Lunar Planet. Sci. Conf. 7th*, 315–335.
- Morris, R. 1978. The surface exposure (maturity) of lunar soils: Some concepts and I<sub>s</sub>/FeO compilation. *Proc. Lunar Sci. Conf. 9th*, 2287–2297.
- Nawa D. F., and J. A. Philpotts 1979. A lunar differentiation model in light of new chemical data on Luna 20 and Apollo 16 soils. In *Regolith from the Highland Region of the Moon* (V. L. Barsukov, Ed.), pp. 336–344. Nauka Press, Moscow.
- Opanasenko, N. V., and Yu. G. Shkuratov 1998. Colorimetry of the Moon in IR-range. *Sol. Syst. Res.* **32**, 1–9.
- Opanasenko, N. V., Yu. G. Shkuratov, D. G. Stankevich, and V. G. Kaydash 1996. Colorimetric mapping of the visible hemisphere of the Moon. *Sol. Syst. Res.* **30**, 352–361.
- Pieters, C. 1977. Characterization of lunar mare basalt types. II. Spectral classification of fresh mare craters. *Proc. Lunar. Sci. Conf. 8th*, 1037–1048.
- Pieters, C. 1978. A summary of spectral reflectance data. *Proc. Lunar Sci. Conf. 9th*, 2825–2849.
- Pieters, C., and T. McCord 1976. Characterization of lunar mare basalt types. *Proc. Lunar Sci. Conf. 7th*, 2677–2690.
- Ryder, J., H. G. McEwen, and U. B. Marvin 1977. Basalts from Mare Crisium. *Moon* **17**, 263–287.
- Shkuratov, Yu. G. 1987. A model of spectral albedo dependence for solid surface of cosmic bodies. *Kinematika. i Fiz. Nebesnykh Tel* **3**, 39–45. [in Russian]
- Shkuratov, Yu. G., N. V. Opanasenko, and M. A. Kreslavsky 1992. Polarimetric and photometric properties of the Moon: Telescope observation and laboratory simulation. 1. *Icarus* **95**, 282–299.
- Shkuratov, Yu. G., D. G. Stankevich, N. V. Opanasenko, V. G. Kaydash, and N. V. Bondarenko 1997. Relationship between albedo and color index of the Moon. *Sol. Syst. Res.* **31**, 41–49.
- Shkuratov, Yu., L. Starukhina, H. Hoffmann, and G. Arnold 1999. A model of spectral albedo of particulate surfaces: Implication for the optical properties of the Moon. *Icarus* **138**, 235–246.
- Soderblom, L. A., J. R. Arnold, J. M. Boyce, and R. P. Lin 1977. Regional variations in the lunar maria: Age, remanent magnetism, and chemistry. *Proc. Lunar Planet. Sci. Conf. 8th*, 1191–1199.
- Taylor, S. 1972. *Lunar Science: Post Apollo Era*. Pergamon, New York.